analytical chemistry

Article

pubs.acs.org/ac

Bimetallic Nanoparticles for Arsenic Detection

Nafiseh Moghimi,[†] Mamata Mohapatra,[†,‡] and Kam Tong Leung*[,†]

[†]Department of Chemistry, University of Waterloo, Waterloo, Ontario, Canada N2L3G1

[‡]Department of Hydro & Electro Metallurgy, Institute of Minerals and Materials Technology, Council of Scientific & Industrial Research, Bhubaneswar 751 013, Odisha, India

Supporting Information

ABSTRACT: Effective and sensitive monitoring of heavy metal ions, particularly arsenic, in drinking water is very important to risk management of public health. Arsenic is one of the most serious natural pollutants in soil and water in more than 70 countries in the world. The need for very sensitive sensors to detect ultralow amounts of arsenic has attracted great research interest. Here, bimetallic FePt, FeAu, FePd, and AuPt nanoparticles (NPs) are electrochemically deposited on the Si(100) substrate, and their electrochemical properties are studied for As(III) detection. We show that trace amounts of As(III) in neutral pH could be determined by using anodic stripping voltammetry. The synergistic effect of alloying with Fe leads to better performance for Fe-noble metal NPs (Au, Pt, and Pd) than pristine noble metal NPs (without Fe alloying). Limit of detection and linear range are obtained for FePt, FeAu, and FePd NPs. The best performance is found for FePt NPs with a limit of detection of 0.8 ppb and a sensitivity of 0.42 μA ppb^{-1}. The selectivity of the sensor has also been tested in the presence of a large amount of Cu(II), as the most detrimental interferer ion for As detection. The bimetallic NPs therefore promise to be an effective, high-performance electrochemical sensor for the detection of ultratrace quantities of arsenic.

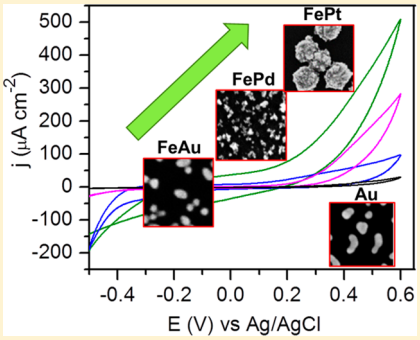

Arsenic (As) is a widely distributed element in nature, as the 20th most abundant mineral in the earth's crust and the 12th most abundant mineral in the human body. Arsenic occurs in organic and inorganic species with oxidation states of −3, +3, and +5.[1,2] Inorganic As is more toxic than organic As, while arsenite (As with a +3 oxidation state) is more toxic than arsenate (As with a +5 oxidation state).[3] In accordance with the World Health Organization[4] and the U.S. Environmental Protection Agency,[5] the acceptable level for maximum As contamination in drinking water is 10 ppb. Drinking water with a higher level of As contamination will cause adverse health effects, including hyperkeratosis on the palm or feet, fatigue, cancer of the bladder, and genotoxic and mutagenic effects.[6] Analytical techniques capable of determining ppb or sub-ppb levels of As are therefore very important for this critical public health threat.[7,8] Electrochemical techniques, particularly stripping voltammetry, are very attractive because of their unique capability for high selectivity for As(III), rapid analysis, and low-cost instrumentation. They also offer high sensitivity and a very low limit of detection comparable to those found in more expensive techniques, such as atomic absorption and inductively coupled plasma spectrometry.[9,10] Furthermore, the generation of very toxic AsH_3(g) as required in most of these latter techniques is not necessary in electrochemical techniques.[11]

Metallic films and nanomaterials have been used as sensing materials for the electrochemical analysis of trace metal ions, including Hg, Cd, Sb, Pb, Fe, and Cu.[12−15] The detection of As in contaminated water with these electrochemical methods has become more popular.[16−20] Bimetallic nanostructured materials, alloy or core−shell nanoparticles (NPs), have attracted much recent attention because of their novel catalytic, magnetic, and optical properties, which could offer significant additional advantages over those of their constituent single-metallic materials. While studies on the sensing properties of bimetallic NPs have been recently reported,[21−23] very few have focused on trace metal detection by electrodes modified by bimetallic or alloy NPs.[24,25] For instance, Gong et al. used Au−Pt inorganic−organic hybrid nanocomposite-modified glassy carbon electrode to detect Hg(II) with a high sensitivity that is not affected by intereference from other metal ions.[24] Lan et al. employed a Au−Pd NP-modified glassy carbon electrode to determine As(III) and reported a detection limit of 0.25 ppb at pH 4.5.[25] However, there is no systematic study on the detection of metal ions by using different bimetallic NPs. Driven by the need for low-cost catalysts and sensors, the study of bimetallic NPs, including inexpensive materials such as Fe, has become a very important research area. Since most of the electrodes employ noble metals (Au and Pt), with and without modification, mixing these noble metals with a low-cost element will not only reduce the production cost but also introduce new properties or enhancement in sensing properties not found in single-metal materials. Here, we report the synthesis of FeM NPs (where M is a noble metal: Pt, Pd, Au) and determine their structural and electrochemical properties. We also evaluate and compare their sensing performance of

Received: November 4, 2014
Accepted: May 4, 2015
Published: May 4, 2015

DOI: 10.1021/ac504116d
Anal. Chem. 2015, 87, 5546−5552

As(III) with those for AuPt NPs (involving two noble metals), and Au, Pd, and Pt pristine NPs (single noble metals). Using anodic stripping voltammetry, we compare the sensitivity and limit of detection of different bimetallic NPs for As(III) detection and obtain the best sensitivity and limit of detection for FePt NPs. We also investigate the interference of Cu(II) ions, which is one of the most serious problems in arsenic detection for these NPs.

EXPERIMENTAL SECTION

Materials and Methods. The chemicals (all analytical grades): $FeCl_2$, $FeCl_3$, $H_2PtCl_6{\cdot}xH_2O$, $AuCl_3$, $PdCl_2$, and $CuCl_2{\cdot}2H_2O$ were purchased from Sigma-Aldrich and used as delivered. The phosphate buffer saline solution (PBS, 0.1 M Na_2HPO_4−NaH_2PO_4−KCl, pH 7.2) was prepared by dissolving PBS tablets (Sigma) in filtered deionized water (18 MΩ cm). Acetate buffer solutions with the desired pH were obtained by mixing appropriate portions of 0.1 M acetic acid and 0.1 M sodium acetate. The Si substrates (15 × 2.5 mm^2, 0.4 mm thick) were cut from an one-side-polished Si(100) wafer (p-type, B-doped, with a resistivity of 0.01−0.02 Ω cm) purchased from Siegert Wafer GmbH. Arsenic stock solution was obtained by dissolving 0.95 g As_2O_3 in 10 mL NaOH (1 M), as per the reaction: $As_2O_3 + 2NaOH \rightarrow 2NaAsO_2 + H_2O$, and diluting the solution to a 100 mL final volume. The pH of the resulting solution was 6, and the concentration of As(III) was 0.048 M. An electrochemical station (CH Instruments 660A) was employed for synthesis and electrochemical analysis, using a three-electrode cell with the NPs deposited on the Si substrate as the working electrode, and a Pt wire and a standard Ag/AgCl electrode as the respective counter and reference electrodes. The background current was recorded for all sweep rates, and it was appropriately removed in calculating the peak currents. The analyte solution was purged with N_2 for 20 min before recording the voltammograms. The surface morphology of the NPs was characterized by field-emission scanning electron microscopy (SEM) in a Zeiss Ultra Plus microscope, and their crystal structures were determined by glancing-incidence X-ray diffraction (XRD) at an incidence angle of 0.5° in a PANalytical X'Pert Pro MRD diffractometer with Cu Kα (1.542 Å) radiation. Chemical-state composition was analyzed by X-ray photoelectron spectroscopy (XPS) as a function of Ar ion sputtering time in a Thermo-VG Scientific ESCALab 250 Microprobe, equipped with a monochromatic Al Kα X-ray source (1486.6 eV). Fabrication of the electrodes is described in the Supporting Information.

RESULTS AND DISCUSSION

Morphology and Composition of Bimetallic NP Electrodes. The SEM images in Figure 1 show that the NPs so obtained generally have a spherical shape with a narrow size distribution and an average size under 100 nm: AuPt (40 nm), FePt (100 nm), FePd (20 nm), FeAu (20 nm), Pd (20 nm), and Au (30 nm). We also obtained pristine Pt NPs (not shown). As these Pt NPs were found to have two different size distributions and they were not very homogeneous, we have therefore not examined them further for the present sensing application. For the largest NP obtained here, the FePt NPs appear to have a rough surface and they consist of grains that are a few nanometers in size. It should be noted that we have determined, in separate experiments, the optimum conditions for the deposition of each NP sample on the Si substrate, and

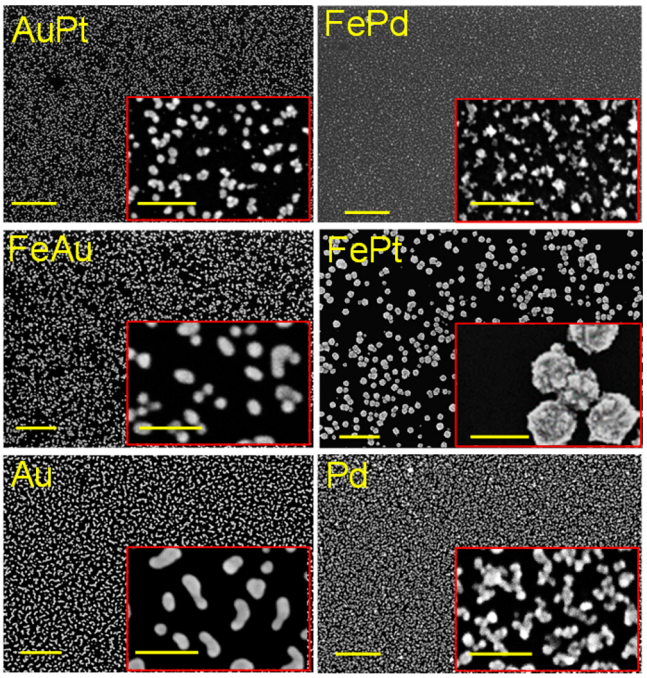

Figure 1. SEM images of $Au_{45}Pt_{55}$, $Fe_{70}Pd_{30}$, $Fe_{40}Pt_{60}$, and $Fe_{10}Au_{90}$ bimetallic NPs and pristine Au and Pd NPs and their higher magnification images in the insets, with scale bars of 500 and 100 nm, respectively.

these conditions were used to prepare the NP samples (shown in Figure 1). For instance, AuPt NPs were obtained by potentiostatic amperometry at −0.8 V for 30 s. Applying a higher potential for the same deposition time did not change the number density nor the size of the NPs, but the deposition became increasingly disrupted due to H_2 evolution. Deposition for a longer time would result in larger NPs with more agglomeration. FeAu and FePd NPs were deposited for 30 s at −1.2 and −1.4 V, respectively. These bimetallic NPs required a more negative applied potential than that for AuPt NPs, because a less negative potential did not produce any deposition. The applied potential could be made even more negative to −1.6 V, but these more negative applied potentials did not lead to very homogeneous deposits, with NPs becoming more distorted in shape and more widely distributed in size.

The relative composition of each sample has been estimated by energy-dispersive X-ray analysis. AuPt NPs are found to correspond to $Au_{45}Pt_{55}$ (i.e., with 45% Au and 55% Pt), which is similar to the ratio of their composition in the electrolyte. In contrast, the compositions of FeM (M = Pt, Pd, and Au) NPs are relatively different from their respective compositions in the electrolytes. We obtain $Fe_{70}Pd_{30}$, $Fe_{40}Pt_{60}$, and $Fe_{10}Au_{90}$ for the compositions of the respective FeM NPs. The relative Au and Pt contents in these FeM NPs are much more than the relative compositions in their respective electrolytes, because their reduction potentials are lower than that for Fe, and their adsorption and reduction rates are therefore much higher than those for Fe[26,27] at the relatively large negative applied potential of −1.4 V (vs Ag/AgCl). For Pd deposition, the number of free ions is reduced in the electrolyte because of the tendency of Pd to stay in the complex form of K_2PdCl_4.

Figure 2a shows the corresponding XRD patterns for FePt, AuPt, FeAu, Au, FePd, and Pd NPs, along with the reference

DOI: 10.1021/ac504116d
Anal. Chem. 2015, 87, 5546−5552

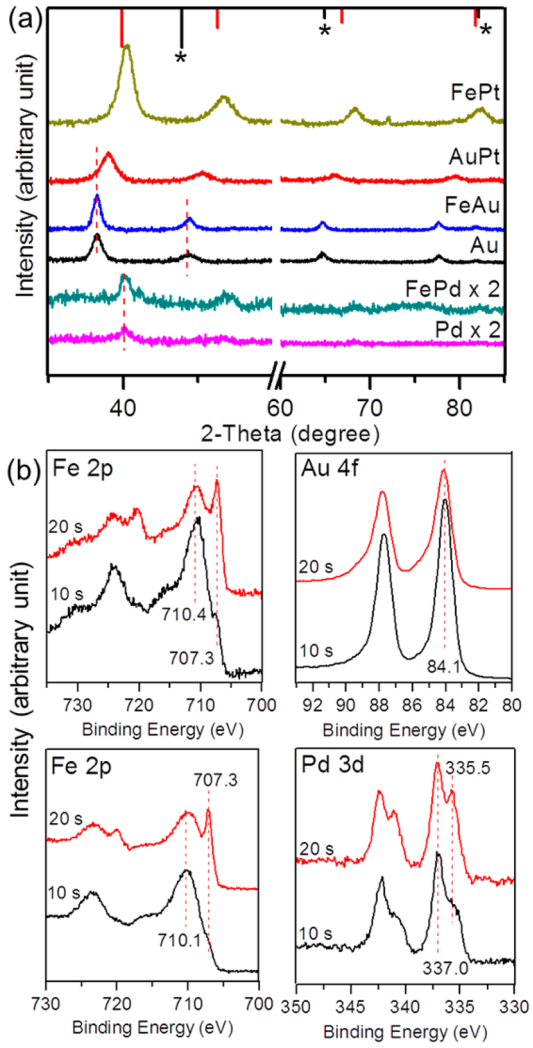

Figure 2. (a) X-ray diffraction patterns of FePt, AuPt, FeAu, and FePd NPs, compared with those of pristine Au and Pd NPs. Reference patterns for Pt (PDF2 00-004-0802) and Fe (PDF2 01-085-1410) are indicated on top by lines and lines with stars, respectively. (b) XPS spectra of Fe 2p and Au 4f regions for FeAu nanoparticles (upper panels) and of Fe 2p and Pd 3d regions for FePd nanoparticles (lower panels), after 10 and 20 s of Ar^+ sputtering.

patterns for Pt (PDF 00-004-0802) and Fe metals (PDF 01-085-1410). As the region of 2-theta = 50−60° contains mainly diffraction features of the Si(100) substrate, this region is therefore not shown. Comparison of the patterns for bimetallic NPs with the pristine metal patterns reveals discernible shifts toward higher 2-theta values for FePt and AuPt NPs than the respective Pt and Au patterns, which indicate lattice expansion as a result of alloy formation. No peak corresponding to pristine Fe in these FePt or FeAu NPs is observed in their respective patterns, which shows that these FePt or FeAu NPs are single phase. The FeAu and FePd patterns exhibit no obvious shift, and they only appear slightly more crystalline, when compared with those of their respective pristine Au and Pd NPs. To confirm alloy formation and the absence of segregated Fe or Au or Pd NPs or domains inside the NPs, we collected XPS spectra of the Fe 2p and Au 4f regions for FeAu NPs and of the Fe 2p and Pd 3d regions for FePd NPs. To identify the peak locations and the corresponding chemical shifts, we fitted the spectra with Gaussian−Lorentzian line-shapes after appropriate correction with the Shirley background. To remove the carbonaceous layer commonly found due to sample handling in air, we performed Ar sputtering of the as-prepared samples for 10 s. We also removed the oxide part of NPs by sputtering for an additional 10 s, which allowed us to study the metallic part of the NPs. Figure 2b shows the resulting chemical-state compositions for typical FeAu and FePd NPs after 10 and 20 s of sputtering. Compared to the pristine Fe XPS features (not shown here), the Fe $2p_{3/2}$ peaks at 707.3 eV has a discernible shift of 0.3 eV toward higher binding energies for both FeAu and FePd NPs. While no obvious difference in the Au $4f_{7/2}$ peak position for the FeAu NPs from the pristine Au is observed, the metallic Pd $3d_{5/2}$ peak for the FePd NPs exhibits a 0.4 eV shift to a higher binding energy. The corresponding Fe $2p_{3/2}$ peaks near 710.4 eV for FePd NPs and 710.1 eV for FeAu NPs are related to the Fe oxides, while the Pd $3d_{5/2}$ peak at 337.0 eV corresponds to Pd silicide. These chemical shifts from the binding energies of the pristine NPs further confirm alloy formation.

Electrochemical Behaviors of Bimetallic-NPs/Si Electrodes. To investigate electrochemical sensing using the as-prepared bimetallic-NP-coated Si electrode, cyclic voltammetry (CV) was carried out in quiescent solutions in a PBS solution with and without arsenic at a scan rate of 50 mV s^{-1}. The electrode was vigorously rinsed with deionized water after each measurement. As an initial evaluation, we compare the CV data of pure Fe NPs with one of the bimetallic NP electrodes (e.g., FePd NPs). Since FePd NPs show much higher current density compared to pristine Fe NPs in a solution containing 1 mM As (Figure S1 of the Supporting Information), we compare all bimetallic NPs only with pristine noble metals. The CV curves from −0.5 to +0.6 V of the AuPt, FePt, FePd, FeAu, Pd, and Au NPs/Si electrodes with and without 1 mM As in a 10 mM PBS solution are shown in Figure S2 of the Supporting Information. The scans were limited to below 0.7 V to prevent the oxidation of NP surfaces. The bare Si electrode has also been used but it was found to exhibit no current response in the presence of As, and it is therefore not shown in Figure S1 of the Supporting Information. In the pristine PBS solution (i.e., without As addition), all NPs/Si electrodes except for the Au and FeAu NPs show a peak near −0.3 V. This peak disappears in the presence of As in the solution, which corresponds to oxidation of As(0) to As(III). Furthermore, a rise in current density at 0.6 V can be observed when As is added to the solution, which can be attributed to oxidation of As(III) to As(V) at a potential above 0.6 V. For the FeAu NPs/Si electrode, no obvious peak corresponding to oxidation of As(0) to As(III) is observed, but the current signal for As(III) oxidation to As(V) is notable. In Figure 3, we compare the current signals obtained from all the electrodes in the presence of As in the solution. The current rise near 0.6 V is found to be the largest for FePt NPs followed by FeAu NPs, but the reduction in current at −0.3 V is the largest for FePd NPs.

To study the effects of different electrolytes and of the pH of the electrolyte on the sensing properties, aqueous solutions of 1 mM As(III) in various media with different pH were prepared and used for CV studies. We have chosen FePt and FeAu NP-coated Si electrodes that exhibit the best primary responses, and we compare the corresponding oxidation currents of As(III) to As(V) in PBS with pH 7, and in acetate buffer solutions with pH 5 (acetic-5) and pH 6 (acetic-6) in Figure 4. Evidently, both FePt and FeAu NPs show similar CV profiles in PBS and acetate buffer solutions in the absence of As, with two

DOI: 10.1021/ac504116d
Anal. Chem. 2015, 87, 5546−5552

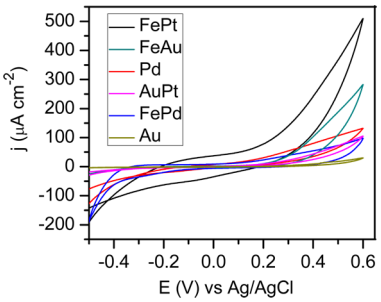

Figure 3. Cyclic voltammograms of FePt, FeAu, Pd, AuPt, FePd, and Au NP-coated Si electrodes (from top to bottom at 0.6 V) in 10 mM PBS and 1 mM As solution. Scan rate is 50 mV s^{-1}.

weak peaks near −0.2 V and +0.1 V in the CV profile of FePt NPs (Figure 4c) compared to that of FeAu NPs (Figure 4a). In the presence of As(III), the current signals for both FePt (Figure 4d) and FeAu NPs (Figure 4b) in PBS are higher than the respective current signals in both acetate buffers. Lowering the pH in the acetate buffer apparently decreases the current response. For the remaining experiments, we have therefore chosen PBS as the optimal electrolyte. Clearly, a neutral pH is particularly important for the practical use of the sensor for drinking water.

Anodic Stripping Voltammetric Detection of Arsenic. Stripping voltammetric techniques are well-known for trace metal analysis providing detection limits comparable to those of very expensive spectroscopic techniques.[1,28,29] The process includes two main steps: electrochemical deposition of trace metals on the electrode (accumulation step), followed by oxidation of the metal back into solution in a linear or pulsed reverse scan (stripping step). Various solutions containing different concentrations of As were prepared and used for these studies. The accumulation step was achieved with the reduction of As(III) to As(0) on the electrode, while the stripping step involved the reverse process (i.e., oxidation). Square wave voltammetry (SWV) and differential pulse stripping voltammetry (DPSV) were carried out using the FePt, FeAu, and FePd NP-coated Si electrodes. Although the As(III) to As(V) oxidation peaks for FePt and FeAu NPs are considerably stronger than that for FePd NPs, the As(0) to As(III) oxidation peak for FePd NPs is larger than those for FePt and FeAu NPs (Figure S2 of the Supporting Information). We have therefore carried out SWV and DPSV measurements for these three samples and calculated their limits of detection. After purging with N_2 gas for 20 min, different amounts of As(III) ions were added step-by-step to the blank test solution. In order to obtain reproducible results, we also applied a constant potential of 0 V (vs Ag/AgCl) for 60 s and stirred rigorously after each stripping step. This also helped to clean and maintain the electrode in its original condition. All electrodes exhibited good stripping signals. Figure 5 (upper panels) shows the SWV curves of FePt and FeAu NPs and DPSV curves of FePd NPs in 10 mM PBS with As(III) increasing from 1 to 3, 5, 10, and 15 ppb after background subtraction. For the preliminary results, SWV and DPSV have been carried out with an accumulation potential of −0.4 V and an accumulation time of 60 s. The solution was stirred throughout the accumulation period, followed by 30 s of equilibrium (rest) time without any stirring before the stripping step. To optimize the current signal, we varied the initial scanning potential, accumulation time, and pH of the electrolyte. The initial scanning potential is an important parameter because it controls both the peak potential and peak current in the stripping voltammogram. We have carried out SWV for FePt with different initial potentials from −0.5 to −0.2 V and obtained the peak current for each potential. When the initial potential was set to −0.4 V, the corresponding current signal increased by 37% compared to that obtained with an initial potential of −0.5 V. Decreasing the initial potential to −0.3 V did not change the current signal, but setting the initial potential to −0.2 V produced a current signal almost twice that obtained with −0.5 V. We have therefore chosen −0.4 V as the

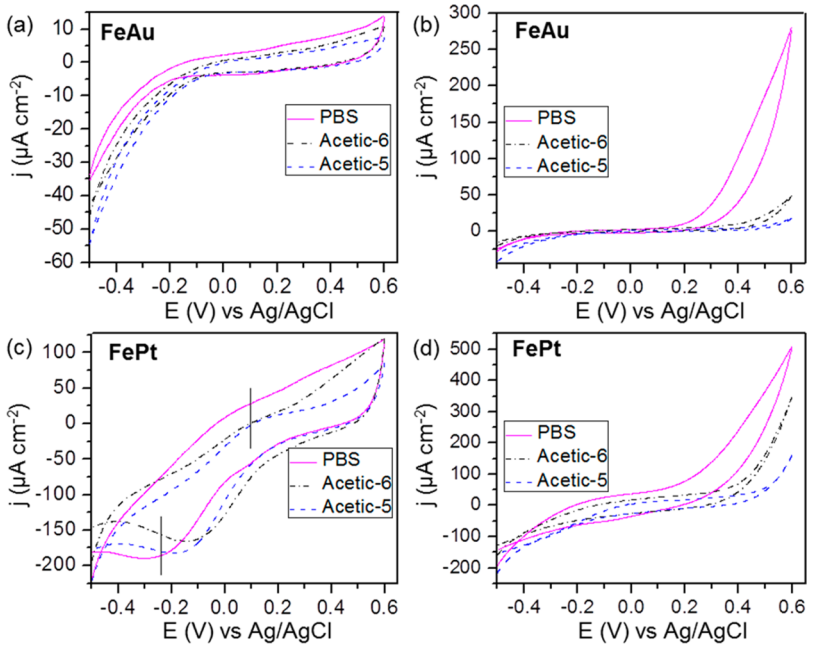

Figure 4. Cyclic voltammograms of (a and b) FeAu and (c and d) FePt NP-coated Si electrodes in 10 mM PBS with pH 7 and in 100 mM acetate buffer solutions with pH 6 (acetic-6) and 5 (acetic-5) (a and c) in the absence and (b and d) presence of As(III). Scan rate is 50 mV s^{-1}.

DOI: 10.1021/ac504116d
Anal. Chem. 2015, 87, 5546−5552

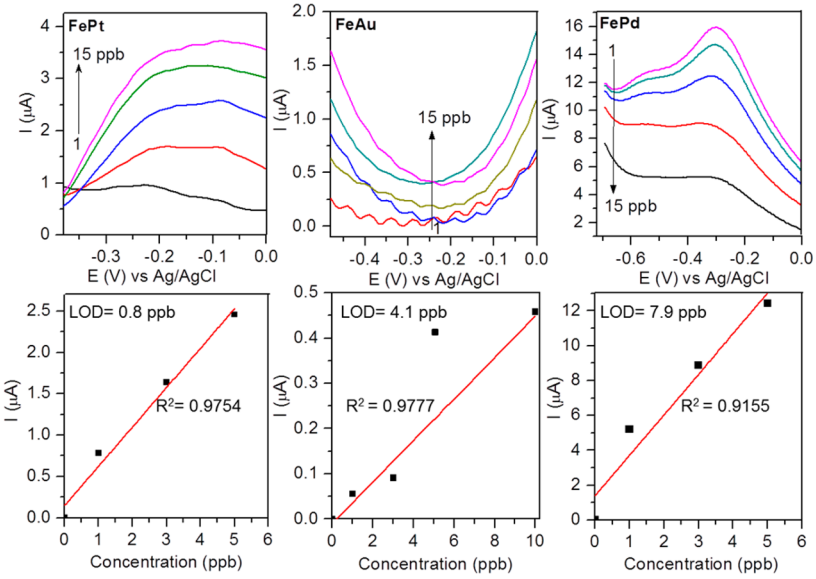

Figure 5. (Top) Square wave stripping voltammograms (SWV) of FePt and FeAu NPs and differential pulse stripping voltammetry (DPSV) of FePd NPs in 10 mM PBS for As(III) concentration of 1, 3, 5, 10, and 15 ppb. The predisposition conditions are −0.4 V and 60 s. (Bottom) The corresponding linear relationships between the peak currents for FePt (at −0.17 V), FeAu (at −0.25 V), and FePd (at −0.3 V), and the As(III) concentration. The limit of detection (LOD) is also given for each of the fitted lines.

Table 1. Comparison of Sensor Performance for Detection of As(III) between the Proposed FePt NP-Coated Si Sensor with Other Sensors Reported in the Literature

sensor	method	electrolyte	linear range (ppb)	limit of detection (ppb)	ref
Au NPs on glassy carbon electrode	linear sweep voltammetry	1 M HCl	0.38−9	0.0096	17
Au-coated Fe_3O_4 on glassy carbon electrode	SWV	0.1 M PBS (pH 5)	0.01−1	0.00097	31
Au NPs on polyaniline film or glassy carbon electrode	SWV	1 M HCl	610−3050	0.4	32
Pt NPs on glassy carbon electrode	linear sweep voltammetry	0.1 M H_2SO_4	0.075−3.75	2	33
Ag NPs on carbon nanotubes coated on glassy carbon electrode	DPSV	1 M HNO_3	10−100	1.20	34
AuPd on glassy carbon electrode	anodic stripping voltammetry	0.1 M acetate buffer solution	1−25	0.25	25
FePt NPs on Si	SWV	0.01 M PBS (pH 7)	1−5	0.8	This work

optimum initial potential because −0.2 V was too close to the peak potential in the SWV curves, which might introduce a false reading in the current signal. We varied the accumulation time from 20 to 120 s and found that an accumulation time of 60 s would give the optimum response. To determine the best pH for the electrolyte, we prepared three different PBS solutions with pH of 3.3, 5.5, and 7 and carried out SWV in these electrolytes. The current signals obtained for oxidation of both As(III) to As(V) and As(0) to As(III) were found to be the highest at pH 7, and they became smaller with decreasing pH. The optimum pH value was therefore set to 7, which serendipitously makes this sensor very environment-friendly and reduces the problems associated with operating in a low pH condition. The optimization for DPSV on FePd NPs followed the same approach used for SWV (data not shown). Using the optimized conditions so determined, increasing the As(III) concentration results in an increase in the respective current signals for FePt and FePd NPs, while the trend from FeAu NPs is less clear, as shown in Figure 5 (top panels). As shown in Figure 5 (bottom panels), a linear fit between the peak current at −0.17 V for FePt, −0.25 V for FeAu, and −0.3 V for FePd and the As(III) concentration in the range of 1−15 ppb is obtained for these NPs. For FePt and FePd NPs, the fits are found to be not very linear over the entire range. We therefore perform these fits over a shorter range of 1−5 ppb. For FeAu NPs, a linear fit can be obtained in the range of 1−10 ppb, by excluding the 5 ppb data point. Among these three NP-coated Si electrodes, FePt NPs exhibit the best limit of detection of 0.8 ppb, which is calculated by $3\sigma/S$, where σ is the standard deviation of 10 blank measurements and S is the slope of the calibration curve. The limits of detection are found to be higher for FeAu (4.1 ppb) and FePd NPs (7.9 ppb). For the FePt NPs with the best (i.e., smallest) limit of detection, the sensitivity of FePt NPs is estimated to be 0.42 μA ppb^{-1}. In Table 1, we compare the sensing performance data of the FePt NPs-coated Si electrode with those for other metallic NPs on different electrodes. It should be noted that our electrode employs the Si substrate for NPs deposition, in contrast to other electrodes that use glassy carbon substrates. Despite the lower conductivity of Si relative to glassy carbon, the present electrode offers competitive sensing performance. In addition, an important advantage of the present sensor is the neutral electrolyte environment (with pH 7), in marked contrast to other sensors that require electrolytes with lower pH. This is particularly important for the practical use of sensors targeted for drinking water. The LOD obtained in this work for metal

DOI: 10.1021/ac504116d
Anal. Chem. 2015, 87, 5546−5552

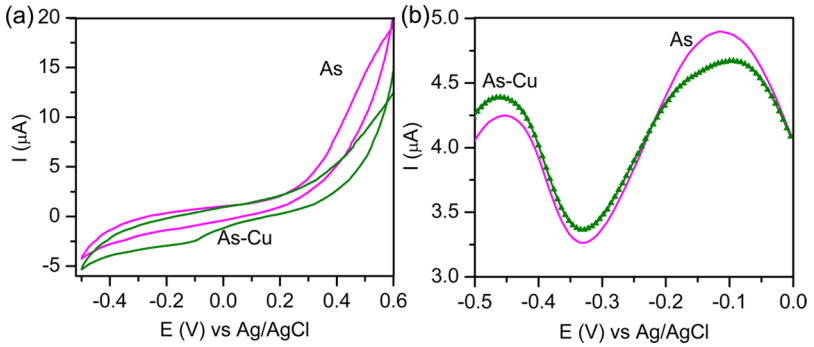

Figure 6. (a) Cyclic voltammograms (scan rate 50 mV s^{-1}) and (b) differential pulse stripping voltammograms of FePt NPs in 10 mM PBS and 15 ppb As(III) with and without 170.5 ppm of Cu(II).

NP-modified electrodes is higher (i.e., worse) than some of the commercially available electrodes [e.g., hanging mercury drop electrode (0.6 ppb)],[30] but it is well within the acceptable range for useful detection of trace amounts of arsenic.

Interference and Stability Studies. Determination of As(III) using anodic stripping voltammetry is known to be susceptible to interferences from various metals.[31,35,36] These interferences arise from either competition for deposition sites on the electrode surface or formation of intermetallic compounds with As during the deposition step.[37,38] Among all the possible interference metals,[30] copper [in the form of Cu(II)] presents the most serious challenge to arsenic detection[33] because its stripping voltage is similar to (and slightly more positive than) the As(III) oxidation voltage. Moreover, Cu can also form intermetallic compounds with As(III) during the deposition process.[39]

Figure 6a shows the CV curves obtained in 10 mM PBS with 15 ppb As(III) solution in the absence and presence of 1 mM of $CuCl_2$, representing 170.5 ppm of Cu(II). Evidently, a decrease in the current signal for the As(III) to As(V) oxidation at 0.5 V and a small change in the region of As(0) to As(III) oxidation at −0.1 V are observed when the Cu(II) ions are present. Since these changes are rather small, we conduct more detailed examination using DPSV to detect any minute change in As(III) in the presence of Cu(II). DPSV curves were obtained after accumulation for 60 s at −0.4 V starting from −0.7 to 0 V in 6 mV increments and with the amplitude (0.05 V), pulse width (0.05 s), sampling width (0.017 V), and pulse period (0.2 s) kept constant. Figure 6b shows the corresponding DPSV curves of FePt NPs in the absence and presence of 170.5 ppm of Cu(II). No discernible change in the detection region of As(III) (i.e., at −0.33 V) is found between the curves, after appropriate background subtraction. There is, however, a discernible decrease in current at −0.11 V in the presence of Cu(II), which can be attributed to Cu oxidation. The present DPSV result therefore shows that Cu(II) oxidation does not interfere with As(III) oxidation, both of which can be detected simultaneously. In our previous work, we have shown that the surface atoms of FePt bimetallic NPs have more d-vacancies than pure Pt NPs.[40] Enhancement in the d-vacancies improves the adsorption and oxidation of the adspecies. Bimetallic FePt NP-modified electrode shifts the oxidation potential of As(0) to As(III) to a more positive potential (i.e., −0.13 V vs Ag/AgCl), while the oxidation potential for Cu(0) to Cu(II) is shifted to a more negative potential (i.e., −0.3 V vs Ag/AgCl). This makes bimetallic NP-modified electrodes more sensitive and selective to As detection.

For the stability test, we have stored the sensors in a drybox at room temperature for an extended period of time and repeated the tests. Only 5% decrease was observed in the current signal after 30 days, which shows the remarkable stability of these sensors (Figure S3 of the Supporting Information).

CONCLUSIONS

Driven by the need for low-cost catalysts and sensors, the incorporation of inexpensive materials such as Fe into active noble metals promises a new approach of synthesizing the next-generation catalysts. In the present work, we obtain bimetallic AuPt, FePt, FePd, and FeAu NPs by electrochemical deposition from the appropriate solutions on the Si(100) substrate. Their morphologies and structures are studied, and their electrochemical properties are optimized to obtain the best bimetallic NPs for As(III) detection. Their As(III) sensing performance, including the sensitivity and limit of detection, are characterized systematically and compared with those of pristine Au, Pd, and Pt NPs by using very precise anodic stripping voltammetry methods, including square wave voltammetry and differential pulse stripping voltammetry. Among the bimetallic NPs studied here, FePt NPs are found not only to provide the best performance, with minimal interference from Cu(II), but also to exhibit long-term stability.

ASSOCIATED CONTENT

Supporting Information

Details for electrode fabrication, CV scans for comparison of different electrodes, and data for the electrode stability test. This material is available free of charge via the Internet at http://pubs.acs.org/.The Supporting Information is available free of charge on the ACS Publications website at DOI: 10.1021/ac504116d.

AUTHOR INFORMATION

Corresponding Author

*E-mail: tong@uwaterloo.ca.

Notes

The authors declare no competing financial interest.

ACKNOWLEDGMENTS

This work was supported by the Natural Sciences and Engineering Research Council of Canada.

REFERENCES

(1) Mays, D. E.; Hussam, A. *Anal. Chim. Acta* **2009**, *646*, 6−16.

DOI: 10.1021/ac504116d
Anal. Chem. 2015, 87, 5546−5552

(2) Chouhan, S.; Flora, S. J. S. *Indian J. Exp. Biol.* **2010**, *48*, 666−678.
(3) Yokel, R. A.; Lasley, S. M.; Dorman, D. C. *J. Toxicol. Environ. Health, Part B* **2006**, *9*, 63−85.
(4) World Health Organization, Arsenic in Drinking Water, Fact Sheet No 372, http://www.who.int/mediacentre/factsheets/fs372/en/index.html.
(5) Natural Resources Defence Council. http://www.nrdc.org/water/drinking/arsenic/aolinx.asp, 2000.
(6) Mandal, B. K.; Suzuki, K. T. *Talanta* **2002**, *58*, 201−235.
(7) Chakraborti, D.; Rahman, M. M.; Paul, K.; Chowdhury, U. K.; Sengupta, M. K.; Lodh, D.; Chanda, C. R.; Saha, K. C.; Mukherjee, S. C. *Talanta* **2002**, *58*, 3−22.
(8) Smedley, P. L.; Kinniburgh, D. G. *Appl. Geochem.* **2002**, *17*, 517−568.
(9) Manisankar, P.; Vedhi, C.; Selvanathan, G.; Arumugam, P. *Microchim. Acta* **2008**, *163*, 289−295.
(10) Muñoz, E.; Palmero, S. *Talanta* **2005**, *65*, 613−620.
(11) Hussam, A.; Alauddin, M.; Khan, A. H.; Rasul, S. B.; Munir, K. M. *Environ. Sci. Technol.* **1999**, *33*, 3686−3688.
(12) Aragay, G.; Pons, J.; Merkoçi, A. *Chem. Rev.* **2011**, *111*, 3433−3458.
(13) Pinilla Gil, E.; Ostapczuk, P. *Anal. Chim. Acta* **1994**, *293*, 55−65.
(14) Mandil, A.; Idrissi, L.; Amine, A. *Microchim. Acta* **2010**, *170*, 299−305.
(15) Zong, P.; Nagaosa, Y. *Microchim. Acta* **2009**, *166*, 139−144.
(16) Baron, R.; Šljukić, B.; Salter, C.; Crossley, A. .; Compton, R. G. *Russ. J. Phys. Chem. A* **2007**, *81*, 1443−1447.
(17) Dai, X.; Nekrassova, O.; Hyde, M. E.; Compton, R. G. *Anal. Chem.* **2004**, *76*, 5924−5929.
(18) Sanllorente-Méndez, S.; Domínguez-Renedo, O.; Arcos-Martínez, M. J. *Electroanalysis* **2009**, *21*, 635−639.
(19) Dai, X.; Compton, R. G. *Anal. Sci.* **2006**, *22*, 567−570.
(20) Xu, H.; Zeng, L.; Xing, S.; Shi, G.; Chen, J.; Xian, Y.; Jin, L. *Electrochem. Commun.* **2008**, *10*, 1893−1896.
(21) Li, W.; Kuai, L.; Qin, Q.; Geng, B. *J. Mater. Chem. A* **2013**, *1*, 7111.
(22) Liu, S.; Zhang, C.; Yuan, L.; Bao, J.; Tu, W.; Han, M.; Dai, Z. *Part. Part. Syst. Charact.* **2013**, *30*, 549−556.
(23) Yan, J.; Liu, S.; Zhang, Z.; He, G.; Zhou, P.; Liang, H.; Tian, L.; Zhou, X.; Jiang, H. *Colloids Surf., B* **2013**, *111C*, 392−397.
(24) Gong, J.; Zhou, T.; Song, D.; Zhang, L.; Hu, X. *Anal. Chem.* **2010**, *82*, 567−573.
(25) Lan, Y.; Luo, H.; Ren, X.; Wang, Y.; Liu, Y. *Microchim. Acta* **2012**, *178*, 153−161.
(26) Oskam, G.; Long, J. G.; Natarajan, A.; Searson, P. C. *J. Phys. D: Appl. Phys.* **1998**, *31*, 1927−1949.
(27) Papadimitriou, S.; Tegou, A.; Pavlidou, E.; Armyanov, S.; Valova, E.; Kokkinidis, G.; Sotiropoulos, S. *Electrochim. Acta* **2008**, *53*, 6559−6567.
(28) Edwards, C. A. *Anodic Stripping Voltammetry: A Review*; Stevenage Laboratory: Hertfordshire, England, 1976; Vol. *22*.
(29) Simm, A. O.; Banks, C. E.; Compton, R. G. *Anal. Chem.* **2004**, *76*, 5051−5055.
(30) Luong, J. H. T.; Lam, E.; Male, K. B. *Anal. Methods* **2014**, *6*, 6157.
(31) Cui, H.; Yang, W.; Li, X.; Zhao, H.; Yuan, Z. *Anal. Methods* **2012**, *4*, 4176.
(32) Chowdhury, A.; Ferdousi, S.; Islam, M. M.; Okajima, T. *Appl. Polym. Sci.* **2007**, *104*, 1306−1311.
(33) Dai, X.; Compton, R. G. *Analyst* **2006**, *131*, 516−521.
(34) Prakash, S.; Chakrabarty, T.; Singh, A. K.; Shahi, V. K. *Electrochim. Acta* **2012**, *72*, 157−164.
(35) Cavicchioli, A.; La-Scalea, M. A.; Gutz, I. G. R. *Electroanalysis* **2004**, *16*, 697−711.
(36) Jena, B. K.; Raj, C. R. *Anal. Chem.* **2008**, *80*, 4836−4844.
(37) Feeney, R.; Kounaves, S. P. *Anal. Chem.* **2000**, *72*, 2222−2228.
(38) Feeney, R.; Kounaves, S. P. *Talanta* **2002**, *58*, 23−31.
(39) Dai, X.; Compton, R. G. *Electroanalysis* **2005**, *17*, 1835−1840.
(40) Moghimi, N.; Leung, K. T. *Anal. Chem.* **2013**, *85*, 5974−5980.

DOI: 10.1021/ac504116d
Anal. Chem. 2015, 87, 5546−5552